

## **EFFECTS OF SUB-FILTER SCALE TURBULENCE MODELS ON VERTICAL VELOCITY STRUCTURE IN NEUTRAL BOUNDARY-LAYER FLOW**

Francis L. Ludwig<sup>1</sup>, Fotini Katopodes Chow<sup>2</sup>, Robert L. Street<sup>1</sup>

1. Stanford University, Stanford, CA  
 2. University of California, Berkeley, CA

### **I. Introduction**

Large eddy simulation (LES) is valuable for studying atmospheric behavior on scales of several tens to hundreds of meters because it treats fine scale motions realistically without requiring impossibly costly computations. The smaller scales are treated as bulk effects at resolved scales to reduce computations. Accurate representation of the small scale is key to successful simulations. Most LES studies have measured success by comparing major simulated flow features with those observed in the field or laboratory. More comprehensive evaluations compare spatial or temporal average profiles of basic state parameters or, sometimes, derived scalar quantities such as divergence, turbulent kinetic energy (TKE), momentum fluxes and so forth. For lack of adequate data, these latter comparisons are generally limited to simple idealized flows, or comparisons of the results obtained with different models. These approaches are appropriate first steps in the study of LES performance, but do not address important questions about measures other than the mean. Under many circumstances, especially for stably-stratified flows, the intermittent processes represented by the spread of the statistical distributions can be an important determinant of the heat, kinetic energy and momentum fluxes. As will be shown, the patterns formed by the vertical motions are also important.

We compare results among six different sub-filter models after a very long spin-up time. These studies address the simple neutrally-stratified flow over a flat surface that Chow et al. (2005) used to evaluate the effects of different models on mean profiles and other statistics. The flow has been well studied theoretically and in the laboratory, so there are norms available for comparison, at least for the mean flow. We describe variations in the flow-field fluctuations observed in LES with different subfilter scale-turbulence models. The Advanced Regional Prediction System (AARPS) mesoscale model was used in an LES configuration to simulate neutrally-stratified flow over a flat, rough surface using six different sub-filter

scale models (Smagorinsky, dynamic Wong-Lilly, and a dynamic reconstruction model with various types and levels of reconstruction). Past work indicated that the dynamic reconstruction model (DRM) results are significantly better than those from traditional eddy-viscosity closure models (e.g. Smagorinsky) when mean velocity profiles are in better agreement with the logarithmic profile of similarity theory. Vertical shear profiles and turbulent stress profiles are also improved by the DRM over traditional models (Chow et al. 2005).

Simulations provide full, consistent data sets for analysis, and development of analysis techniques. Different flow parameters, and a variety of statistical measures can be used to characterize and compare results. This work presents the variations in the fluctuations observed in vertical velocities generated by LES of turbulent flows when the sub-filter scale models are changed.

### **2. Flow simulation examined**

#### **2.1 ARPS model**

ARPS is a state of the art atmospheric mesoscale and small-scale finite difference simulation code that can be applied to LES problems (Xue et al., 1995, 2000, 2001). Chow et al. (2005) modified ARPS to include new sub-filter scale models for this study. Its most relevant properties as used in this work are summarized in Table 1. ARPS winds are computed on the faces of the grid volumes; *u* on the west and east, *v* on the south and north and *w* on the bottom and top, and interpolated to the computational volume centers (where temperatures and pressures are also defined) for output, display and analysis. The vertical spacing in Table 1 refers to the original staggered grid. Parameter values from nine separate *snapshots* at 2500 s intervals, beginning at 280 000 s were used for the analyses reported here. The spin up of more than 3 days simulated time would be expected to provide a statistically steady state, but Chow et al. (2005) showed that even after these long integration times, results were not completely stationary (see e.g.

---

<sup>1</sup> corresponding author: Francis L. Ludwig, Environmental Fluid Mechanics Laboratory, Stanford University, Stanford, CA 94305-4020, phone: 650-725-5948, fax: 650-725-9720, e-mail: fludwig@stanford.edu

their Figure 2), because of inertial oscillations and hence differing numbers of larger scale structures within the domain. The 2500 s between samples should provide independent data that can be combined for calculating statistics for model comparisons. All comparisons involve only data from the same height above the surface, because of the large vertical gradients in the flow.

Table 1. Characteristics of ARPS as used for tests

| Characteristic                        | Description  |
|---------------------------------------|--|
| Spatial discretization                | Arakawa C grid                                       |
| Number of grid points                 | 40x40x40   |
| Horizontal spacing                    | 32 m   |
| Vertical spacing for the computations | Stretched: 10 m near surface, 65 m near top (1500 m) |
| Time discretization: Large step       | 0.5 s, 2nd-order leapfrog                            |
| Small step (acoustic mode)            | 0.05 s, 1st-order fwd-bckwd                          |
| Horizontal advection                  | Fourth order   |
| Vertical advection                    | Second order   |
| Boundaries: Bottom                    | Rigid free slip with sfc drag                        |
| Top                                   | Rigid free slip                                      |
| Lateral                               | Periodic   |
| Spatial computational mixing          | Fourth order   |
| Subfilter-scale turbulence            | Discussed in Section 3                               |

## 2.2 Test case: Neutral atmospheric boundary layer

The simulations used for the comparisons given here are described by Chow et al. (2005). A similar neutral, rotation-influenced, large-scale boundary layer flow was examined by Andren et al. (1994). A constant pressure gradient drives the flow; it corresponds to a  $10 \text{ m s}^{-1}$  westerly geostrophic wind at approximately  $43^\circ$  north latitude. The simulation was initialized with small perturbations superimposed on the analytical (constant eddy-viscosity) Ekman spiral solution, so that fully turbulent flow developed. The parameterized surface fluxes approximate a rough lower boundary.

## 3. Sub-filter scale turbulence models tested

Chow et al. (2005) implemented reconstruction approaches for the resolved subfilter stresses, modeled the subgrid stresses, and added a model for near-wall effects at rough boundaries. For the readers' convenience, we give a brief overview of the models.

LES uses the equations of motion to describe the evolution of larger scale motions directly, while modeling smaller scale eddies, most often by representing their effects as analogous to viscosity. For this approach to work, energy in the unresolved scales must be small enough that they are not the major forcing in the evolution of larger scales. The size that separates the larger, resolved scales from smaller, unresolved scales is for practical (not necessarily physical) reasons related to the size of the mesh used to represent the flow, so the mesh should be fine enough that most of the flow energy is resolved — the underlying basis for LES. Key to all the following discussions is that both resolved sub-

filter scale (RSFS) and sub-grid scale (SGS) models must use only knowledge of resolved scale behavior.

When derivatives are estimated from a spatial array of point values (rather than in an infinitesimal volume) for numerical solution of the equations of motion, the discretization acts as a spatial filter. This implicit discretization filter and the explicit LES filter divide flow energy into three categories: 1) wholly resolved motions, 2) motions at scales resolved by the grid, but smoothed by the filtering and 3) wholly unresolved motions. Motions in category 2 are known as resolved sub-filter-scale (RSFS) motions. If a known explicit filter is used, RSFS motions can be reconstructed mathematically and used to model their effects on resolved motions. RSFS motions cannot always be reconstructed exactly, because of numerical limitations in the process. Chow et al. (2005) combined both the Taylor series RSFS reconstruction model of Katopodes et al. (2000a, b) and the Stolz and Adams' (1999) approximate deconvolution approach with the Wong and Lilly (1994) dynamic eddy viscosity model to form a dynamic reconstruction model (DRM). Unresolved sub-filter scales (USFS) must always be modeled (Gullbrand and Chow, 2003).

The filtered, incompressible Navier-Stokes equations on a discrete mesh are:

$$\frac{\partial \bar{u}_i}{\partial t} + \bar{u}_j \frac{\partial \bar{u}_i}{\partial x_j} = -\frac{1}{\rho} \frac{\partial \bar{p}}{\partial x_i} - g \delta_{i3} + \varepsilon_{imn} f_n \bar{u}_m - \frac{\partial \bar{\tau}_{ij}}{\partial x_j} \quad (1)$$

$$\frac{\partial \bar{u}_i}{\partial x_j} = 0 \quad (1a)$$

Repeated indices indicate summation; viscous terms have been neglected. Tildes and over-bars denote discretization and filtering effects, respectively. Wind components and coordinate axes are denoted by subscripted  $u$  and  $x$ , respectively. Other symbols are: pressure,  $p$ ; Coriolis parameter,  $f$ ; gravitational constant,  $g$ ; Kronecker delta,  $\delta_{ij}$  and the alternating epsilon tensor,  $\varepsilon_{imn}$ . Turbulent stresses are defined:

$$\tau_{ij} = \overline{u_i u_j} - \bar{u}_i \bar{u}_j \quad (2)$$

Carati et al. (2001) separated stress into two parts representing: 1) the subgrid stress that depends on unresolved motions (USFS), and 2) sub-filter stress that depends on differences between the exact and filtered motions (RSFS). Theoretically, exact values of the RSFS component could be reconstructed from filtered fields. Separating USFS and RSFS stress in Equation 2 gives:

$$\tau_{ij} = \left( \overline{u_i u_j} - \bar{u}_i \bar{u}_j \right) + \left( \bar{u}_i \bar{u}_j - \bar{u}_i \bar{u}_j \right) \quad (3)$$

Following the example of Carati et al. (2001)  $\bar{A}_{ij}$  is used to represent USFS (the first parenthesis on the right side of Equation 3) and  $B_{ij}$  to represent RSFS (second parenthesis). The complete models require a term representing the USFS components in  $\bar{A}_{ij}$ , because  $\overline{u_i u_j}$  cannot be calculated from grid point values. A reconstruction term is also needed for

RSFS motions and associated stresses in  $B_{ij}$ . Chow et al. (2005) used six different model combinations in ARPS to simulate the neutral boundary layer flow described earlier.

### 3.1 Eddy viscosity subgrid-scale models

The eddy velocity concept is widely used in LES, and has been adopted here for the SGS models tested. The basic form for representing the subgrid component is:

$$\bar{A}_{ij} = -2\nu_T \bar{S}_{ij} = -\nu_T \left( \frac{\partial \bar{u}_i}{\partial x_j} + \frac{\partial \bar{u}_j}{\partial x_i} \right) \quad (4)$$

where  $\nu_T$  is the SGS eddy viscosity, and  $\bar{S}_{ij}$  is the resolved strain rate tensor. Equation 4 requires the determination of eddy viscosity. Two models are tested below: 1) the Smagorinsky model and 2) the dynamic Wong-Lilly model.

#### 3.1.1 Smagorinsky model

The original Smagorinsky (1963) model approximates eddy viscosity  $\nu_T$  as proportional the local resolved strain and the square of the grid spacing  $\Delta_g^2$ :

$$\nu_T = (C_S \Delta_g)^2 (2\bar{S}_{ij}\bar{S}_{ij})^{1/2} \quad (5)$$

The Smagorinsky model without any sub-filter scale term,  $B_{ij}$ , provides baseline results against which results from more complete models can be compared.

#### 3.1.2 Dynamic Wong-Lilly model

The dynamic Smagorinsky model (Germano et al., 1991) is overly sensitive to the bottom boundary condition, so the dynamic Wong and Lilly (DWL, 1994) model was adopted. It is less sensitive to the bottom boundary than the dynamic Smagorinsky model (Germano et al. 1991) and relatively easy to implement. The DWL model defines eddy viscosity as:

$$\nu_T = C_S^{2/3} \Delta^{4/3} \varepsilon^{1/3} = C_\varepsilon \Delta^{4/3} \quad (6)$$

$C_S$  and  $\varepsilon$  are the original Smagorinsky coefficient and the turbulent dissipation rate, respectively; they are replaced by  $C_\varepsilon$  as shown in Eq. 6. The Wong-Lilly model avoids the usual requirement that  $\varepsilon$  and the SGS rate of energy production be equal, and it does not require the effective grid cell spacing,  $\Delta$ , to be defined exactly, because the product term,  $C_\varepsilon \Delta$ , is dynamically calculated (Germano *et al.*, 1991) from Lilly's (1992) least squares approximation:

$$C_\varepsilon \Delta^{4/3} \approx \frac{\frac{1}{2} \left\langle L_{ij} \hat{S}_{ij}^c \right\rangle}{\left[ 1 - \left( \frac{\hat{\Delta}}{\Delta} \right)^{4/3} \left\langle \hat{S}_{ij}^c \hat{S}_{ij}^c \right\rangle \right]} \quad (7)$$

Brackets  $\langle \rangle$  indicate local averaging and  $\hat{\cdot}$  denotes application of an explicit filter. The Leonard term stress tensor,  $L_{ij}$ , and the filtered strain rate tensor,  $\hat{S}_{ij}^c$  are:

$$L_{ij} = \overline{\overline{\overline{u_i u_j}}^c} - \overline{\overline{u_i}^c \overline{u_j}^c} \quad (8)$$

and

$$\hat{S}_{ij}^c = \frac{1}{2} \left( \frac{\partial \hat{u}_i^c}{\partial x_j} + \frac{\partial \hat{u}_j^c}{\partial x_i} \right) \quad (9)$$

The effects of the discretization operator at the coarser test-level grid are denoted by  $\sim^c$ . The dynamic Wong-Lilly (DWL) model is less sensitive to calculation of the strain rate tensor near the lower rough boundary and was found to perform better than the dynamic Smagorinsky model (Chow et al. 2005, Germano et al. 1991). The DWL was used alone, and in combination with four different sub-filter reconstruction models. Three reconstruction models represent different levels of reconstruction vis-a-vis the number of terms in the series that were retained.

### 3.2 Sub-filter reconstruction models

The filter operation that results in Equation 1 damps high wave number information. In theory, RSFS information can be recovered exactly with appropriate inverse filtering. Stolz et al. (2001) proposed an approximation to the inverse filtering that uses van Cittert's (1931) iterative method to estimate unfiltered velocities  $\tilde{u}_i$  from the filtered field  $\bar{u}_i$ . Alternatively, Chow and Street (2002) used Taylor series expansions for the purpose. The recovered unfiltered fields,  $\tilde{u}_i$ , are substituted into the RSFS stress tensor,  $B_{ij} = \overline{\tilde{u}_i \tilde{u}_j} - \bar{u}_i \bar{u}_j$ . Truncating the reconstruction at different points provides different models for the RSFS term  $B_{ij}$ . As described above, SGS stresses are provided by modeling the stress term  $\bar{A}_{ij} = \overline{u_i u_j} - \bar{u}_i \bar{u}_j$ .

Both the van Cittert iterative and Taylor series methods recover the velocity to a known order of accuracy. Both low- and higher-order reconstructions were used to model the RSFS stresses with these methods. The expansions are equivalent to the Scale Similarity Model (SSM) of Bardina *et al.* (1983) and Leonard's (1974) tensor-diffusivity model (Katopodes *et al.*, 2000b; Winckelmans *et al.*, 2001) when they are appropriately truncated.

#### 3.2.1 Approximate Deconvolution Model (ADM)

Van Cittert's (1931) iterative deconvolution method retrieves unfiltered quantities by a series of operations with a filter  $G$  as follows:

$$\tilde{u}_i = \bar{u}_i + (I - G)\bar{u}_i + (I - G)((I - G)\bar{u}_i) + \dots ; \quad (10)$$

$I$  is the identity matrix (Stolz et al. 2001) and  $G$  is a smooth spatial filter, here chosen to be a tophat filter. Further details are available in Chow et al. 2005. The truncated series approximates the unfiltered velocity  $\tilde{u}_i^*$  and when substituted gives  $B_{ij} = \overline{\tilde{u}_i^* \tilde{u}_j^*} - \bar{u}_i^* \bar{u}_j^*$ .

Stolz et al. (2001) called this reconstruction the approximate deconvolution model (ADM). Three levels of ADM reconstruction were used for the tests, each with the Wong-Lilly model. A "level- $n$ " reconstruction retains  $n + 1$  terms of the series that approximates the inversion of the filter  $G$ . Our tests use level 0, 1 and 5 reconstructions.

### 3.2.2 Modified Clark reconstruction model

Reconstruction with a Taylor series can be done to an arbitrary order of accuracy in the isotropic filter width  $\Delta_f$ . For example, to fourth order, the expansion gives:

$$B_{ij} = \overline{\tilde{u}_i^* \tilde{u}_j^*} - \bar{u}_i^* \bar{u}_j^* - \frac{\Delta_f^2}{24} \left( \overline{\tilde{u}_i \nabla^2 \tilde{u}_j} - \bar{u}_j \nabla^2 \bar{u}_i \right) \quad (11)$$

Clark et al. (1977) showed that terms with higher order derivatives are dissipative. Katopodes et al. (2000b) rewrote the series model in Equation 11 in the following form that is equivalent to fourth order:

$$B_{ij} = \frac{\Delta_f^2}{12} \frac{\partial \bar{u}_i}{\partial x_m} \frac{\partial \bar{u}_j}{\partial x_m}, \quad (12)$$

which we call the modified Clark model.

### 3.3 Near-wall stress model

The near-wall stress model is implemented to supplement the turbulence models and account for the stress induced by filtering near a solid boundary as well as the effect of the large grid aspect ratio near the lower boundary. This model is based on that of Brown et al. (2001). Essentially, it adds a drag to the flow to account for the roughness and grid aspect ratio effects. The resulting stress appears as

$$\tau_{i, near-wall} = - \int C_c a(z) |u| u_i dz \quad (13)$$

Nakayama and Sakio (2002) and Nakayama et al. (2004) provided a theoretical basis for this near-wall model of rough boundary flow. The shape function  $a(z)$  is chosen so that the near-wall stress tapers smoothly to zero beyond the near-wall region. Chow et al. (2005) defined the coefficient  $C_c$  which ranges between about 0.4 to 0.8, depending on grid cell aspect ratio. The depth of the near-wall stress layer was taken as  $4\Delta x$  (about 128 m).

## 4. Results

We analyzed the differences between distributions of a variety of flow descriptors in space, so

that we could determine if there are differences among the models in the way momentum is transferred in the vertical. Scalar descriptors (e. g., flow velocity, vertical motion, or the spanwise component of vorticity) rather than vectors or tensors make it easier to compare statistical distributions and to display spatial patterns. Among those parameters that are closely related to momentum transfer in the vertical are spanwise vorticity and vertical velocity, both of which are measures of overturning and vertical motions that move momentum (flow velocity) to and from the surface. Had this been other than a neutrally-stratified flow without buoyant effects, Richardson Number and Brunt-Vaisala frequency would have been good choices to examine heat transfer. Although we calculated several of these variables, only the vertical velocity fields will be discussed here. The other parameters, such as spanwise vorticity lead to similar conclusions that will be presented elsewhere.

### 4.1 Temporal variability

Even after  $10^5$  s, Chow et al. (2005) found inertial oscillations between about 0.8 to 1.2 in stationarity parameters that equal one for steady-state conditions (see their Figure 2). One reason why these variations may persist is that the flow is characterized by a few large, coherent structures (e.g. regions of updraft and downdraft) that dominate the statistics of integrated surface stress used to calculate the stationarity parameters. If coherent features are large enough (several hundred meters in extent) so that no more than five or ten features can occupy the domain at any given time, then variations of two or three in their number will produce systematic variations in stationarity parameters, and other statistics. Furthermore, if the size and shape of large coherent structures (if they exist) are different for different models, that would signal that the flows produced by the different models are significantly different in the effects that they produce, such as scalar transport and dispersion. Therefore, it is important to examine more than just differences in mean behavior between models. Other statistics and flow measures could be very important, especially standard deviations and the nature of the spatial distributions of flow variables. Chow (2004) had already found evidence of coherent structures in the spatial correlations of streamwise velocity.

Chow et al. (2004) evaluated the performance of the different models by comparing layer mean velocities and shears with the theoretical logarithmic profile values. They used the non-dimensional velocity gradient

$$\Phi = \frac{\kappa z}{u_*} \sqrt{\left( \frac{\partial \langle \bar{u} \rangle}{\partial z} \right)^2 + \left( \frac{\partial \langle \bar{v} \rangle}{\partial z} \right)^2} \quad (14)$$

In Equation 14,  $u_*$  is friction velocity,  $\kappa$  is the von Kármán constant;  $\Phi$  should be 1 in the logarithmic layer. In the first hundred meters,  $\Phi$  lies between

about 0.99 and 1.06, 1.08 or 1.6, for the DRM-ADM0, Wong-Lilly and Smagorinsky models, respectively, leading the authors to conclude that the Smagorinsky model is the least realistic of those tested, and the ADM-DRM formulations are the most realistic. Here, we accept that hierarchy, and thereby infer that results presented later for the different models are less realistic for the Smagorinsky than for the others.

#### 4.2 Variations of layer averages and standard deviations of vertical velocity with height

Figure 1 shows profiles of vertical velocity standard deviation. The lowest 110 m is plotted separately so the scales can be expanded to allow the differences among models to be seen more readily. Continuity requires that the layer mean vertical velocities (not shown) equal zero, and statistical tests confirmed that none of the layer averages differs significantly from zero, so only standard deviations are shown in Figure 1. Fluctuations in vertical velocity are important to the determination of vertical momentum fluxes. Large standard deviations can be produced by either 1) large organized areas of upward and downward motion, 2) up and down motions randomly distributed over the grid points, or 3) a combination of the two. As will be shown later, it is the first of these that seems to be the most important.

In order to produce velocity profiles with a momentum sink at the surface, there must be downward momentum transport. Downward momentum transport in an LES arises by two mechanisms, 1) direct vertical subgrid transport accomplished by the models being studied, or 2) horizontal subgrid transport between areas of resolved upward and downward motion. In the second case, if there is no interchange between upward and downward moving cells, higher momentum air from aloft eventually returns to its original level with the same momentum. We will return to this idea later when the patterns of vertical motion are discussed.

The standard deviations in Figure 1 have regular and significant variations with height. The largest values occur at about 200 m for all the models. Since the upper and lower boundary conditions fix vertical motions at zero, the standard deviations are forced to approach zero near the top and bottom of the profiles. Differences among  $w$  standard deviations were evaluated at 15 m and 959 m, using the F test (Bluman 2001). All the differences at 959 m are significant at the 95 percent level. The models differed significantly at 15 m in all but one (Modified Clark and DRM\_ADM1) of 15 possible pairings.

Our results have shown that different models often produce significantly different statistical distributions. Here, each  $w$  is associated with a point in space), and although the mean vertical velocities are all statistically indistinguishable from zero and from each other, there may be different patterns of spatial distribution, because of spatial correlations. We next examine the spatial patterns of vertical motion to see if this is in fact the case).

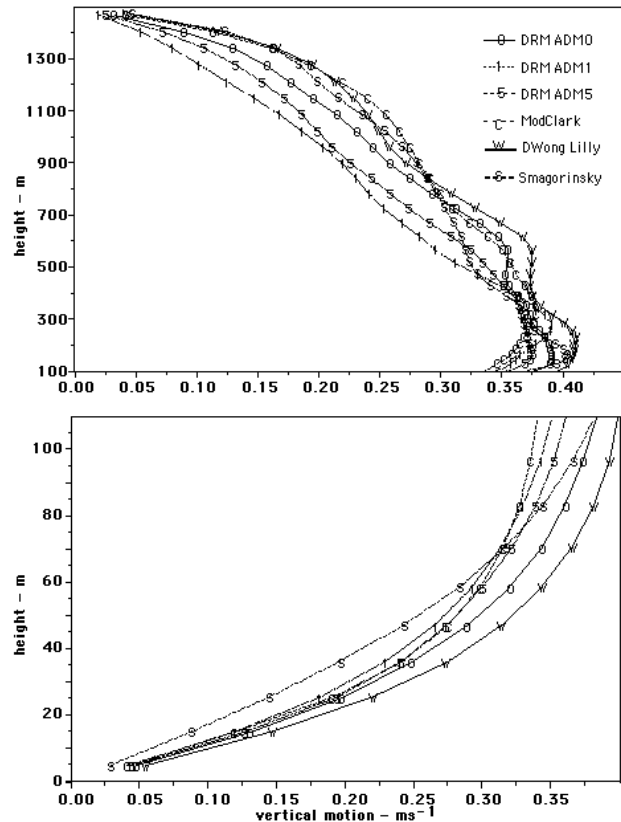


Figure 1. Vertical profiles of layer standard deviation of vertical velocity.

Figures 2 and 3 show vertical motions at 15 m and 517 m above the surface for the six models (the six large squares) at each of the nine snapshot times. Vertical velocities are shown by the color, blues for downward motion, reds for upward. Whites and pale colors are near zero. In Figures 2 and 3, colors range between  $\pm 50 \text{ cm s}^{-1}$  and  $\pm 150 \text{ cm s}^{-1}$ , respectively, although some extremes (upper right corner of each panel) are outside these ranges.

Qualitative differences among the models are obvious in Figure 2. Smagorinsky results differ from those of other models, with upward and downward motions being organized in long stripes at an angle to the west-east geostrophic motion. The Wong-Lilly and DRM\_ADM0 models produce vertical motion patterns arranged in less pronounced tilted stripes. Other model results look more like mosaics of updrafts and downdrafts. Another factor that differentiates Smagorinsky patterns from the others is their generally smaller magnitude. Although extreme values for  $w$  in Figure 2 are not smallest for the Smagorinsky model, the standard deviation profiles in Figure 1 confirm that overall, the Smagorinsky model's vertical motions near the ground deviate less from zero than do other model results.

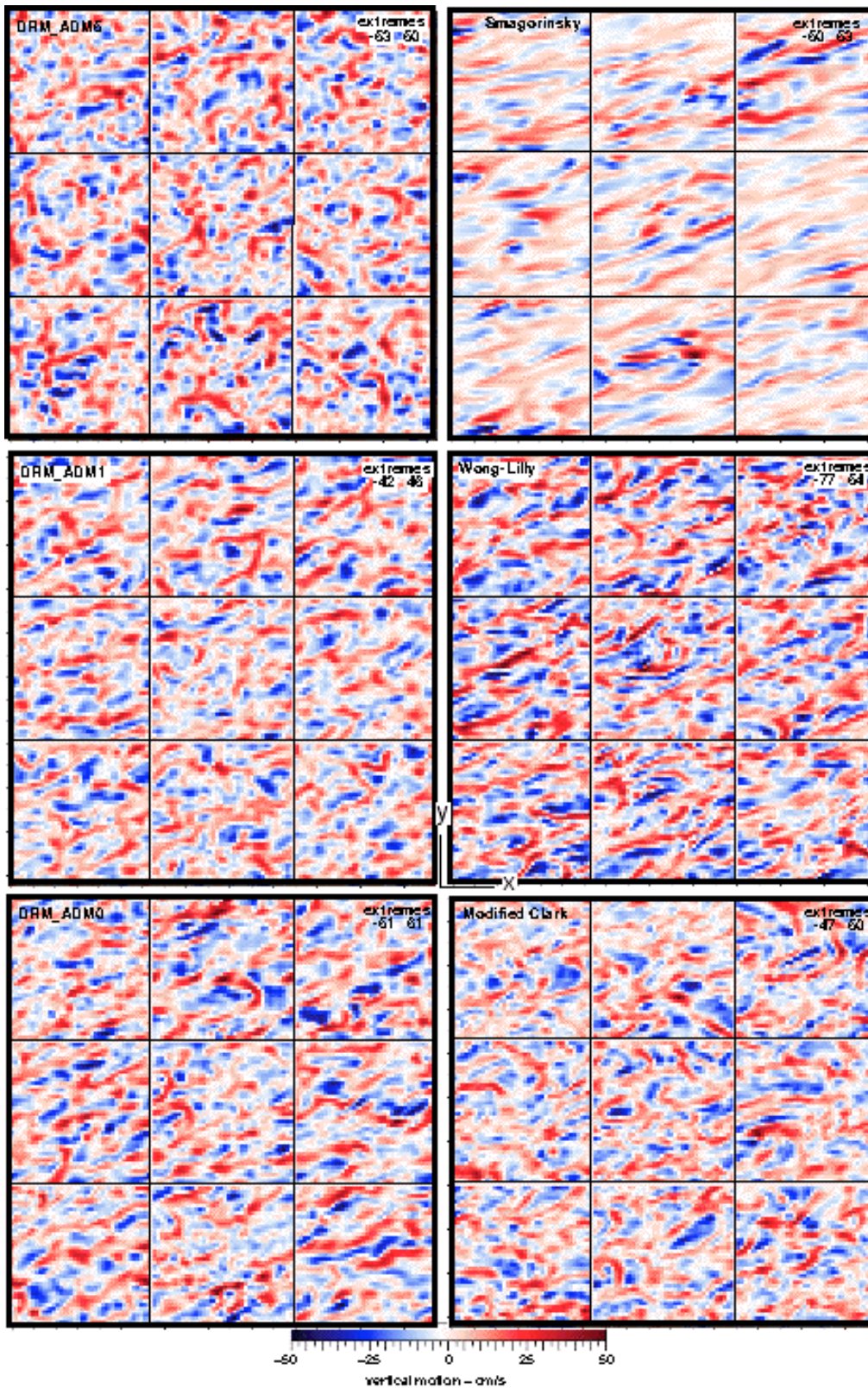


Figure 2 Vertical motions produced at 15 m by the six subfilter models (large squares). The small squares at upper left are the earliest of the nine times for that model; the latest is at the lower right. Extreme values for each model are shown in the upper right corner of each large square.

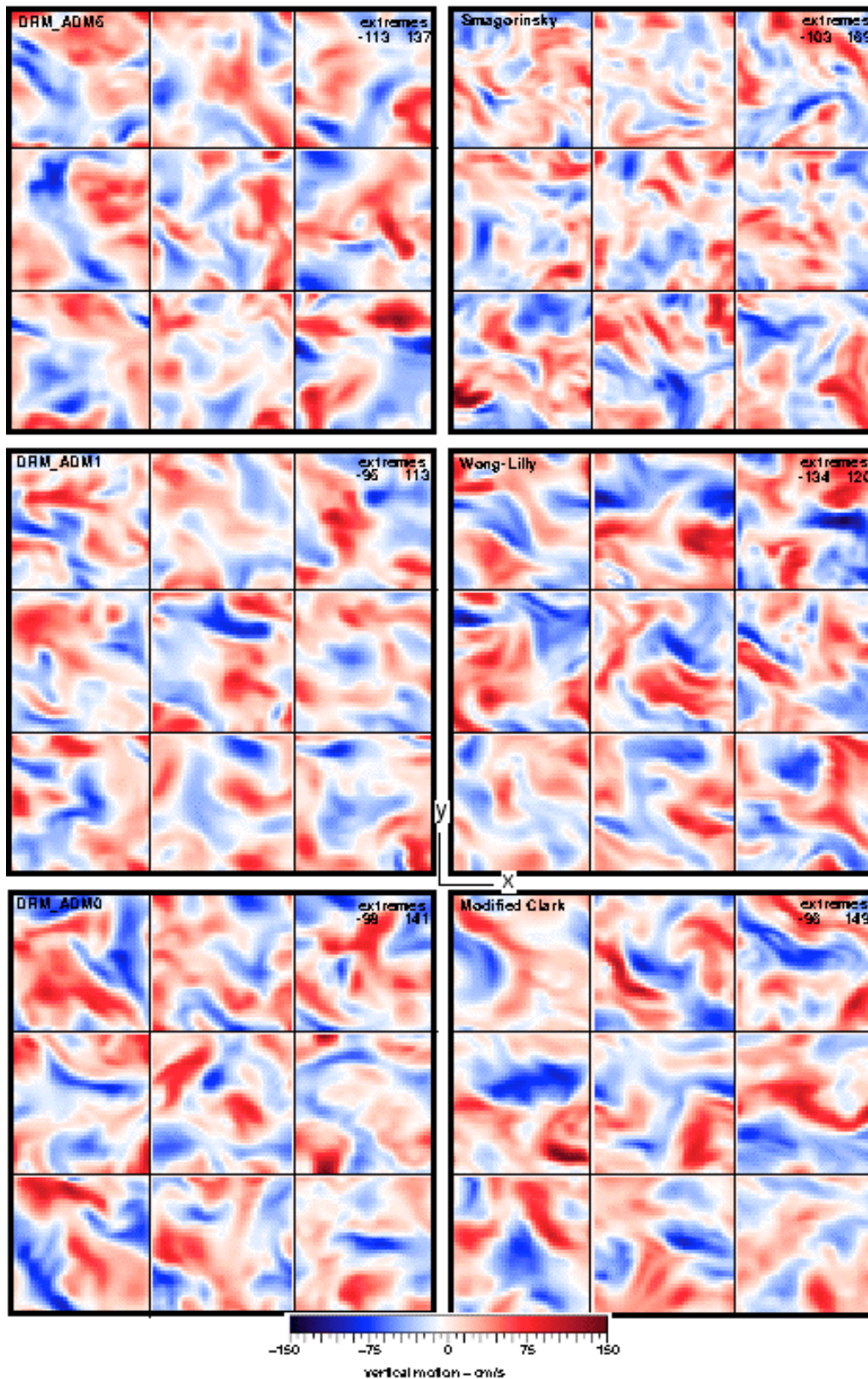


Figure 3 Vertical motions produced at 517 m by the six subfilter models (large squares). The small squares at upper left are the earliest of the nine times for that model; the latest is at the lower right. Extreme values for each model are shown in the upper right corner of each large square. Note: the color scale differs from Figure 10.

Figure 3 shows vertical motions at 517 m; the color scale spans a larger range than in Figure 2. The qualitative differences among the patterns produced by the various models are much less pronounced at this height than they are near the surface. The patterns at 517 m are qualitatively quite different from those at 10 m. The elongations are gone, and the features are much larger. At the higher altitude, the Smagorinsky patterns are not as markedly different from those produced by the other models, but overall, the Smagorinsky features do contain smaller features. The noticeable differences well away from the wall at 517 m are counter to the common belief that the turbulence model is only important near the wall. It appears that errors near the surface affect the entire flow field. Interestingly, Khanna and Brasseur (1998) reached the same conclusion for moderately convective boundary layers.

The correlograms in Figures 4 and 5 confirm that patterns change with height. At 15 m, all the models, except the DRM\_ADM5, produce elongated features with major axes of the area encompassed by the 0.3 correlation that are at least 1.8 times the minor axis (See Table 2). At the higher level, only the Wong-Lilly model has a ratio as high as 1.9. As noted, the upper level features are also larger, especially with regard to the minor axis dimension, which doesn't exceed 105 m at the 15 m height, but is greater than 290 m for all models at 517 m.

Table 2 Vertical velocity correlogram axis lengths and angles for 0.3 correlation isopleths

| Height (m) | Subfilter Model | axis length (m) |       | Major/minor ratio | Major axis angle - degrees |
|------------|-----------------|-----------------|-------|-------------------|----------------------------|
|            |                 | Major           | Minor |                   |                            |
| 15         | DRM_ADM0        | 228             | 90    | 2.55              | 14                         |
| 15         | DRM_ADM1        | 192             | 91    | 2.10              | 19                         |
| 15         | DRM_ADM5        | 145             | 105   | 1.38              | 21                         |
| 15         | ModClark        | 165             | 92    | 1.80              | 6                          |
| 15         | WongLilly       | 216             | 78    | 2.77              | 15                         |
| 15         | Smagorinsky     | 381             | 82    | 4.65              | 12                         |
| 517        | DRM_ADM0        | 446             | 336   | 1.33              | -26                        |
| 517        | DRM_ADM1        | 463             | 297   | 1.56              | -17                        |
| 517        | DRM_ADM5        | 426             | 347   | 1.23              | -36                        |
| 517        | ModClark        | 524             | 335   | 1.56              | -14                        |
| 517        | WongLilly       | 562             | 295   | 1.90              | -19                        |
| 517        | Smagorinsky     | 405             | 357   | 1.13              | -27                        |

Chow (2004) presented correlation diagrams at 5, 111 and 839 m for the magnitude of the u velocity component (instead of w). They are similar to those in Figures 4 and 5. She only examined the Smagorinsky and DRM\_ADM5 model runs. Her Smagorinsky results at 5 m had roughly the same rotation and extent as those in Figure 4. As altitude increased, the u-correlation ellipses rotated CW and the eccentricity decreased. Chow's (2004) DRM\_ADM5 correlograms indicate that the u component features are more elliptical than we see for the w component, but in both cases the size of the features (as indicated by the area enclosed by a given correlation isopleth) increases with altitude.

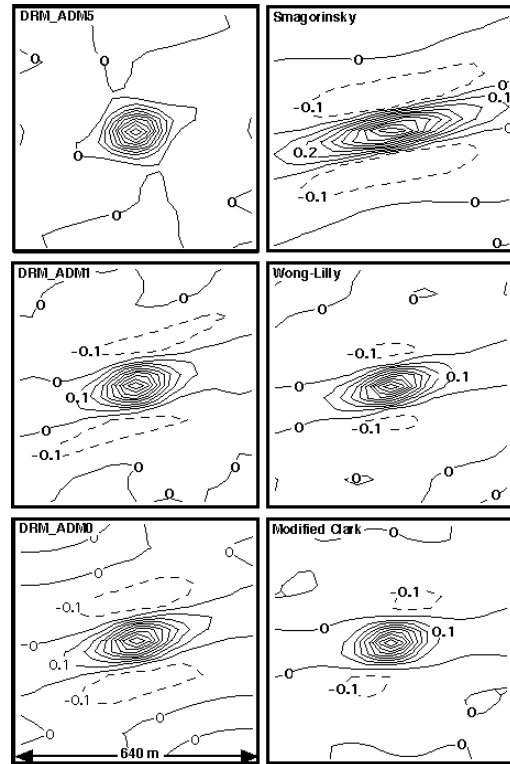


Figure 4. Vertical velocity correlograms at 15 m for the six models. Isopleth interval is 0.1; dashed lines=negative correlations

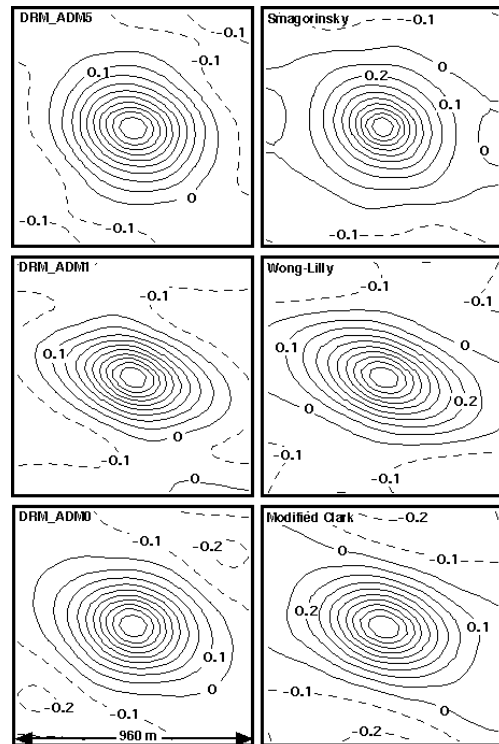


Figure 5. Vertical velocity correlograms at 517 m for the six models. Isopleth interval is 0.1; dashed lines=negative correlations

Kosovic (1997) compared a “linear” model (corresponding to the Smagorinsky used here) and a “non-linear” model (a more accurate model when comparing mean velocity profiles). His  $u$  component correlograms are similar to Chow’s (2004). His linear model produced structures that were more elongated at low levels than those of the more complicated model, but the differences aloft were less at higher levels, where both models produced more nearly circular features. It appears that models of the Smagorinsky type produce elongated features near the surface (at least for  $u$ , and  $w$ ) that become more circular aloft. The more complete models (e.g. DRM\_ADM5) exhibit less difference between the shapes of features at low levels and those aloft. The low level features tend to be nearly as circular as those at higher altitudes. Based on the mean speed profiles, we infer that patterns produced by more complete models are more realistic than those of a Smagorinsky model. This could be very important in some applications, because the transport and dispersion associated with the different patterns are likely to be very different.

Chow (2004) examined the streamwise, normalized one-dimensional energy spectra at different heights above the surface for a similar simulation on a larger  $83^3$  grid and found that at an altitude of 161.5 m, the Smagorinsky model had more energy than the DRM\_ADM0 model, and that the added energy was associated with larger wave numbers, i.e. smaller size features. This differed from the spectra at 5 m, where the DRM\_ADM0 had greater energy at larger wave numbers. This is certainly consistent with the entries in Table 2, which show that the major axes (which are the more closely aligned with the streamwise direction) of the 0.3 correlation isopleths are larger for the Smagorinsky model than for the DRM\_ADM0 at the lower altitude and smaller at the higher level. It appears that differences in spectra among the models can be attributed to differences in the patterns of organized motion produced by the different subfilter models.

The DRM\_ADM5 and Smagorinsky patterns of  $w$  were plotted for all levels (not shown) after 290 000 s of simulation to see how they changed with height. In both cases, the transition to larger features with height takes place largely by the merging of smaller areas of upward or downward motion. The motions become stronger with increasing distance from the lower boundary and its dampening effects. Features evolve with height so that it is often difficult to match patterns separated by more than a few hundred meters in the vertical.

## 5. Summary and discussion

Differences in flow feature variabilities, as measured by horizontal layer standard deviations can have great practical importance, because the intensity of fluctuations has a direct impact on turbulent fluxes of momentum and scalar variables. The fact that the models produce different standard deviations is interesting, but of itself not particularly enlightening. It is important to remember that the standard

deviations seen in the profiles do not derive from randomly distributed spatial distributions of the scalars involved. Instead, as we have shown, there are organized patterns, i.e., a value at any point is likely to be of the same sign and of similar magnitude as its immediate neighbors. These spatial patterns and the correlations associated with them have been shown to be recognizably different for different models, especially at the lower altitudes, but also far above the ground. Based on the extent of the area covered by spatial correlations greater than 0.3 (see Table 2), the patterns will span from about 3 to 20 grid points, depending on altitude and directional orientation. When LES results are used for driving other applications (e.g. transport and dispersion models), the differences in patterns among the models would likely lead to very different results. The question remains, how are these pattern differences associated with the different effects of the various subfilter models? Below, we suggest a possible answer by analogy to what Sreenivasan et al. (1989) observed and theorized about the behavior of constant scalar surfaces in turbulent fluids.

Sreenivasan et al. (1989) related fine scale details of the interfaces between mixing layers to the macroscopic fluxes between layers. The shapes of iso-surfaces (e.g., a surface of constant dye concentration) are made up of convoluted wrinkles on convoluted wrinkles over a range of scales. Over that range of scales, the area of the surface varies according to the resolution ( $R$ ) with which it is measured. The variation in area  $A$  follows a power law of the form:

$$A = CR^{2-D} \quad (15)$$

$C$  is a constant and  $D$  is a fractal dimension with a value of approximately  $7/3$ , meaning that the area increases with finer resolution. The relationship in Equation 15 does not hold over all sizes. At the larger sizes, it is bounded by an outer scale ( $R_o$ ) which is approximated by the integral scale of the turbulence. At this outer scale, the area is  $A_o$ . The small, inner scale bound ( $R_i$ ) is approximated by the Komolgorov scale. The inner scale defines the maximum area for the surface

$$A_{\max} = A_o \left( \frac{R_i}{R_o} \right)^{2-D} \quad (16)$$

Sreenivasan et al. (1989) note that “... *an interesting interpretation* [of the above described behavior] *is that the turbulent surfaces at the ‘microscopic’ level adjust themselves in such a way that the ‘macroscopic’ fluxes are independent of viscosity.*” In essence, Sreenivasan et al. (1989) argue that the transfer of momentum and other scalars is accomplished by microscale processes across the thin layers associated with the wrinkled convoluted surface shapes discussed above. The effect of changing viscosity is to change the small scale cutoff of the fractal behavior of the interfaces, and hence the overall surface area over which the microscale processes are actively mixing the scalars.

Large-eddy simulations present a situation different from that described by Sreenivasan et al. (1989) in that the small-scale end of the cascade is fixed by the filter and/or grid scales. Furthermore, the LES may not produce the fractal interfaces found in real fluids, probably because of the aforementioned fixed small scale. We hope to examine this question in the future. However, the idea that the total surface area may be adjusted to accommodate “viscosity” changes does seem to apply. In LES, differences in the behavior of the subfilter models generate the different “viscosities.” The changes in the shapes of the resolved features are attempts to produce the differences in interface area that are necessary for the proper large scale transfers of momentum in the turbulent flow.

Figure 1 shows that the near-wall average behavior varies substantially from model to model, most pronouncedly for the Smagorinsky model. In these simulations, as noted above, there is a momentum sink at the surface, and a source at altitude. The flow must transfer momentum toward the surface sink. In an effort to properly transfer the momentum to the surface, the greater “viscosity” of the Smagorinsky model introduces patterns that are likely unrealistic. Given the improved agreement with similarity theory for the dynamic reconstruction models, it seems reasonable to assume that the larger-scale, near-surface patterns produced by these other models are more realistic, given their more realistic mean profiles.

Others have found differences in the larger scale patterns produced by different subfilter models. Chow’s (2004) u-component correlograms had much the same elongations as were presented here for the vertical velocity. Kosovic’ (1997) demonstrated that the energy spectrum for his more accurate “nonlinear” model included more small scale, i.e. large wave number, energy. The patterns observed here are consistent with that result. Chow (2004) also found that the DRM-ADM0 simulations have considerably more energy at small scales than do simulations using the Smagorinsky model.

Interestingly, Figures 2 and 3 show that the DRM models stimulate smaller-scale resolved motions near the wall than does the Smagorinsky model; the distinction decreases far from the wall where the eddies are larger, and a significantly larger fraction of the total energy is held in the resolved scales. There, differences among models are less important (cf., Khanna and Brasseur, 1998). Near the wall, the “better” models have a significant impact on the resolved scales and to some degree that impact extends away from the wall. The dynamic models and the reconstruction models allow some backscatter of energy, which mimics the expected interactions of the resolved and subfilter scales (cf., Leslie and Quarini, 1979). However, the DRM-ADM models mimic this process more faithfully, yielding a much more active spectrum in the smaller scales of the resolved flow.

In the future, we expect to apply the EOF analysis techniques described by Ludwig and Street (1995) to see if the patterns reported here are also

detected by the EOF analysis. Ludwig et al. (1996) used EOF methods to compare fractal support dimensions in an observed atmospheric flow and a corresponding LES; the LES patterns were more space-filling than was observed. The various models can be compared as the atmosphere and LES were in that study. Support dimensions are likely related to the shapes of the boundaries between regions of upward and downward motion, and the effectiveness of the various models with regard to transferring energy to the smaller scales. Considering the results presented here, analysis of more complex flows certainly seems warranted (e.g. the stratified flow over Askervein Hill, Chow and Street 2002).

**Acknowledgements.** We gratefully acknowledge the support of National Science Foundation Grant ATM-0453595 (Physical Meteorology Program: S. Nelson, Program Director), and the National Center for Atmospheric Research (sponsored by NSF) for the computing time used in this research.

## References

- Andren, A., A. R. Brown, J. Graf, P. J. Mason, C.-H. Moeng, F. T. M. Nieuwstadt, and U. Schumann, 1994: Large-eddy simulation of a neutrally stratified boundary layer: A comparison of four computer codes. *Quart. J. Royal Meteorol. Soc.*, **120**, 1457-1484.
- Bardina, J., J. H. Ferziger, and W. C. Reynolds, 1983: *Improved turbulence models based on large eddy simulation of homogeneous, incompressible, turbulent flows*. Tech. Report TF-19. Dept. of Mech. Eng., Stanford U., Stanford, CA., 174 pp.
- Bluman, A. G., 2001: *Elementary statistics: a step by step approach, 4<sup>th</sup> ed.*, McGraw-Hill Higher Education, New York, NY, 757 pp.
- Brown, A. R., J. M. Hobson and N. Wood, 2001: Large-eddy simulation of neutral turbulent flow over rough sinusoidal ridges. *Bound. Lay. Meteorol.*, **98**, 411-441.
- Carati, D., G. S. Winckelmans, and H. Jeanmart, 2001: On the modelling of the subgrid-scale and filtered-scale stress tensors in large-eddy simulation. *J. Fluid Mech.*, **441**, 119-138.
- Chow, F. K., 2004: *Sub-filter-scale turbulence modeling for large-eddy simulation of the atmospheric boundary layer over complex terrain*, PhD dissertation, Dept. of Civil and Environ. Eng., Stanford U., Stanford, CA, 339 pp.
- Chow, F. K. and R. L. Street. 2002: Modeling unresolved motions in LES of field-scale flow, *Preprints 15th Symp. Boundary Layers and Turb.*, Amer. Meteorol. Soc., Boston, MA, , 432-435.
- Chow, F. K., R. L. Street, M. Xue and J. H. Ferziger. 2005: Explicit filtering and reconstruction turbulence modeling for large-eddy simulation of neutral boundary layer flow, *J. Atmos. Sci.*, **62**, 2058–2077.
- Clark, R. A., J. H. Ferziger, and W. C. Reynolds, 1977: *Evaluation of subgrid-scale turbulence*

- models using a fully simulated turbulent flow*. Tech. Report TF-9. Dept. of Mech. Eng., Stanford U., Stanford, CA., 119 p.
- Germano, M., U. Piomelli, P. Moin, W. H. and Cabot, 1991: A dynamic subgrid-scale eddy viscosity model, *Phys. of Fluids*, **3**, 1760-1765.
- Gullbrand, J. and F. K. Chow, 2003: The effect of numerical errors and turbulence models in large-eddy simulations of channel flow, with and without explicit filtering. *J. Fluid Mech.*, **495**, 323-341.
- Katopodes, F. V., R. L. Street, and J. H. Ferziger, 2000a: Sub-filter-scale scalar transport for large-eddy simulation. *Preprints 14th Symp. Boundary Layers and Turb.*, Amer. Meteorol. Soc., Boston, MA, 472-475.
- Katopodes, F. V., R. L. Street, and J. H. Ferziger, 2000b: A theory for the sub-filter-scale model in large-eddy simulation. Tech. Report 2000-K1. Environ. Fluid Mech. Lab., Stanford U., Stanford, CA., 19 p.
- Khanna, S. and J. G. Brasseur, 1998: Three-dimensional buoyancy- and shear-induced local structures of the atmospheric boundary layer. *J. Atmos. Sci.*, **55**, 710-743.
- Kosovic', B. 1997: Subgrid-scale modeling for large-eddy simulation of high-Reynolds-number boundary layers, *J. Fluid Mech.*, **336**, 151-182.
- Leonard, A., 1974: Energy cascade in large eddy simulation of turbulent fluid flows, *Advances in Geophys.*, **18A**, 237-248
- Leslie, D. C. and G. L. Quarini, 1979: Application of turbulence theory to the formulation of subgrid modeling procedures, *J. Fluid Mech*, **91**, 65-91.
- Lilly, D. K., 1992: A proposed modification of the Germano subgrid-scale closure method, *Phys. of Fluids*, **4**, 633-635.
- Ludwig, F. L. and R. L. Street, 1995: Modification of multiresolution feature analysis for application to three-dimensional atmospheric wind fields, *J. Atmos. Sci.*, **52**, 139-157.
- Ludwig, F. L., R. L. Street, J. M. Schneider and K. R. Costigan, 1996: Analysis of small-scale patterns of atmospheric motion in a sheared, convective boundary layer, *J. Geophys. Res.*, **101D**, 9391-9411.
- Nakayama, A., Hori, K., and Street, R. L., 2004: Filtering and LES of flow over irregular rough boundary, *Proc. Summer Program 2004*, Center for Turbulence Research, Stanford U., pp. 145-156.
- Nakayama, A. and K. Sakio, 2002: Simulation of flows over wavy rough boundaries, *Annual Res. Briefs*, Center for Turbulence Research, NASA Ames and Stanford University, 313-324.
- Smagorinsky, J. 1963 General circulation experiments with the primitive equations. *Mon. Weather Rev.*, **91**, 99-152.
- Sreenivasan, K. R., R. Ramshankar and C. Meneveau, 1989: Mixing, entrainment and fractal dimensions of surfaces in turbulent flows, *Proc. Roy. Soc. London*, **A 421**, 79-108.
- Stolz, S. and N. A. Adams, 1999: An approximate deconvolution procedure for large-eddy simulation, *Phys. of Fluids*, **11**, 1699-1701.
- Stolz, S., N. A. Adams, and L. Kleiser, 2001: An approximate deconvolution model for large-eddy simulation with application to incompressible wall-bounded flows. *Phys. of Fluids*, **13**, 997-1015.
- van Cittert, P. ,1931: Zum Einfluß der Spaltbreite auf die Intensitätsverteilung in Spektrallinien II., *Zeitschrift für Physik*, **69**, 298-308.
- Winckelmans, G. S., A. A. Wray, O. V. Vasilyev, and H. Jeanmart, 2001: Explicit-filtering large-eddy simulation using the tensor-diffusivity model supplemented by a dynamic Smagorinsky term, *Phys. of Fluids*, **13**, 1385-1403.
- Wong, V. C. and D. K. Lilly, 1994: A comparison of two dynamic subgrid closure methods for turbulent thermal-convection., *Phys. of Fluids*, **6** , 1016-1023.
- Xue, M., K. K. Droegemeier, and V. Wong, 2000: The Advanced Regional Prediction System (ARPS): A multi-scale nonhydrostatic atmospheric simulation and prediction model. Part I: Model dynamics and verification., *Meteorol. and Atmos. Phys.*, **75**, 161-193.
- Xue, M., K. K. Droegemeier, V. Wong, A. Shapiro, and K. Brewster, 1995: *ARPS Version 4.0 User's Guide.*, Center for Analysis and Prediction of Storms, U. of Okla., Norman, OK, 380 p.
- Xue, M., K. K. Droegemeier, V. Wong, A. Shapiro, K. Brewster, F. Carr, D. Weber, Y. Liu, and D. Wang, 2001: The Advanced Regional Prediction System (ARPS): A multi-scale nonhydrostatic atmospheric simulation and prediction tool. Part II: Model physics and applications, *Meteorol. and Atmos. Phys.*, **76**, 143-165.